Bull. Mém. Soc. Anthropol. Paris (2013) 25:1-18
DOI 10.1007/s13219-012-0069-z

ARTICLE / *ARTICLE*

# First description of the Cro-Magnon 1 endocast and study of brain variation and evolution in anatomically modern *Homo sapiens*

## Première description de l'endocrâne de Cro-Magnon 1 et étude de la variation et de l'évolution du cerveau chez les Hommes anatomiquement modernes

**A. Balzeau · D. Grimaud-Hervé · F. Détroit · R.L. Holloway · B. Combès · S. Prima**

Received: 23 May 2012, Accepted: 10 September 2012


**Abstract** Paleoneurology is an important research field for studies of human evolution. Variations in the size and shape of the endocranium are a useful means of distinguishing between different hominin species, while brain asymmetry is related to behaviour and cognitive capacities. The evolution of the hominin brain is well documented and substantial literature has been produced on this topic, mostly from studies of endocranial casts, or endocasts. However, we have only little information about variations in endocranial form, size and shape in fossil anatomically modern *Homo sapiens* (AMH) and about the evolution of the brain since the emergence of our species. One good illustration of this limited knowledge is that one of the first fossil *H. sapiens* discovered, in 1868, that is also one of the oldest well-preserved European specimen has never been studied in what concerns its endocranial morphology. The first aim of this study was to propose a detailed description of the endocranial anatomy of Cro-Magnon 1, using imaging methodologies, including an original methodology to quantify endocranial asymmetries. The second aim was to compare samples of the fossil and extant AMH in order to document differences in the form, size and shape of the endocasts. A decrease in absolute endocranial size since the Upper Palaeolithic was noticeable. Although both extant and older endocrania have the same anatomical layout, we nonetheless found non-allometric differences in the relative size and organization of different parts of the brain. These document previously unknown intraspecific anatomical variations in the *H. sapiens* brain, demonstrating its plasticity, with some areas (frontal and occipital lobes) having been more subject to variation than others (parietal, temporal or cerebellar lobes). That may be due to constraints to maintain an optimal performance while reducing in size and changing in shape during our recent evolution.

**Keywords** Endocasts · *Homo sapiens* · Cro-Magnon · Brain evolution · Paleoneurology · Asymmetry

**Résumé** La paléoneurologie est un champ de recherche important dans le cadre des études sur l'évolution humaine. Les variations de taille et de forme de l'endocrâne sont en effet utiles pour différencier les différentes espèces d'homininés, alors que les asymétries cérébrales sont reliées au comportement et aux capacités cognitives. Pourtant, notre connaissance de l'évolution et de la variation du cerveau d'*Homo sapiens*, depuis l'apparition de notre espèce, est très lacunaire. Dans un premier temps, nous détaillons l'anatomie et les asymétries (en proposant une méthode innovante de quantification de ces dernières) de l'endocrâne de Cro-Magnon 1, un des représentants européens les mieux conservés et les plus anciens des Hommes anatomiquement modernes, qui n'avait encore pu être analysé. Puis, une étude comparative entre un échantillon de spécimens fossiles et actuels d'*Homo sapiens* est effectuée. Bien qu'un substrat anatomique commun soit présent, certaines différences de taille et d'organisation

A. Balzeau (✉) · D. Grimaud-Hervé · F. Détroit
Département de préhistoire du Muséum national d'Histoire naturelle, équipe de paléontologie humaine,
UMR 7194 du CNRS, Paris, France
e-mail : abalzeau@mnhn.fr

R.L. Holloway
Department of Anthropology, Columbia University,
New York NY 10027, USA

B. Combès · S. Prima
Inserm, U746, F-35042 Rennes, France

INRIA, VisAGeS Project-Team, F-35042 Rennes, France

University of Rennes-I, CNRS, UMR 6074, IRISA,
F-35042 Rennes, France

ont été observées entre ces deux échantillons. Ces résultats illustrent la plasticité du cerveau au sein de notre espèce et documentent une variabilité anatomique encore inconnue.

**Mots clés** Endocrânes · *Homo sapiens* · Cro-Magnon · Évolution cérébrale · Paléoneurologie · Asymétrie

## Introduction

Paleoneurology is a major field of research in paleoanthropology, which has produced abundant literature documenting the evolution of the hominin brain [1–3]. However, although we have a fairly good overview of the evolution and variation of endocranial anatomy in the different hominin species during the 7 Ma of human history, and more particularly in the last 3 Ma, our knowledge and understanding of variations and modifications of the brain in anatomically modern *Homo sapiens* (AMH) in the last 200,000 years is very patchy. This is partly due to the limited material available and the small amount of published data about endocasts of fossil *H. sapiens*.

In 1868, five human skeletons, corresponding to four adults and a child, were exhumed in the Cro-Magnon rock shelter located in Les Eyzies-de-Tayac, near the town of Sarlat in Dordogne, France [4–7]. This discovery was of paramount importance at the time: while the antiquity of man was definitely accepted as a fact, these remains were among the first fossil specimens attributed to *H. sapiens*. Anthropologists concluded that they represented a "Cro-Magnon race" [8–10]. This typology is not in use anymore, but the term "Cro-Magnon" is still used in popular science literature, and sometimes by scientists, as a synonym for prehistoric man and/or to refer to anatomically modern fossil *H. sapiens* found in Europe. Since their discovery, several detailed anatomical studies have been performed on the Cro-Magnon fossils [5,6,10–12]. The first individual ("subject No. 1"), initially referred to as the "old man", has also been the focus of many palaeopathology studies because of intriguing macroscopic bone lesions [5,6,10,11,13–15]. The remains unearthed in the Cro-Magnon site were originally attributed to the Aurignacian period but this question has been much debated. Since then, a date of 30,000 BP was first proposed by comparison with the $^{14}C$ dates obtained for the Aurignacian sequence from the Abri Pataud in Dordogne [16]. However, dating of a shell ornament recently found in association with the human remains suggests an age not earlier than 28,000 BP. The burial could therefore be attributed to the Gravettian period [17]. The very good state of preservation of the Cro-Magnon 1 skull made it impossible to reach its internal features, but a detailed study of data obtained from imaging methodologies (CT scans) gave us access to a whole series of internal anatomical structures for this specimen, such as pneumatisation of the facial and temporal bone, cranial vault thickness and structural bone composition, allowing us to supplement previous anatomical descriptions of this specimen (Fig. 1).

We have only little information about variations in endocranial anatomy, size and shape in fossil AMH, and the evolution of the *H. sapiens* brain since the emergence of our species is poorly documented. A gradual and relatively small decrease in absolute endocranial size since the Upper Palaeolithic was previously reported (e.g., [18]). It has been proposed that this trend could "be explained as an allometric decrease based on a loss of bony/muscular robusticity, without any significant behavioural association" [2,19], or could be correlated with a reduction in body size [18]. However, these interpretations lack sufficient demonstration because of the limited data available. More importantly, no information is currently available about a possible correlation between variations in the shape and structure of the brain and this decrease in absolute size. This is an important limitation to recent efforts drawing on developments in brain mapping and computational anatomy in living humans that aim to analyse brain structure and function in order to document variations in the *H. sapiens* brain.

Given this context, this study has two major objectives. The first is to describe the internal cranial anatomy of Cro-Magnon 1, and particularly its endocast, accessed thanks to imaging methodologies. Because of the excellent state of preservation and completeness of the specimen, its endocranial surface has never been casted, and therefore never been studied. Our second aim is to document the differences in form, size and shape of the endocast between extant and anatomically modern fossil *H. sapiens*, using all the fossil specimens available and a very broad sample of extant humans.

## Material

In Africa, the oldest attested AMH are Omo 1 [20] and Herto Bouri [21], aged 195,000 and 154,000 years respectively. Omo 1 is rather incomplete and Herto Bouri has not been exhaustively studied as yet and its endocast has not been described. Then there is a gap in fairly complete African specimens [22] until the Epipaleolithic populations from Afalou-Bou-Rhummel and Taforalt. Moreover, some early African individuals have severe pathological alterations of the vault that could influence the study of their endocranial shape. In addition, some specimens that are sometimes called "archaic" *H. sapiens* have morphological differences with "true" AMH (e.g., [23]). Therefore, we have not considered specimens from these two groups in our study (e.g., Eliye Springs, Jebel Irhoud, Florisbad, Ngaloba,

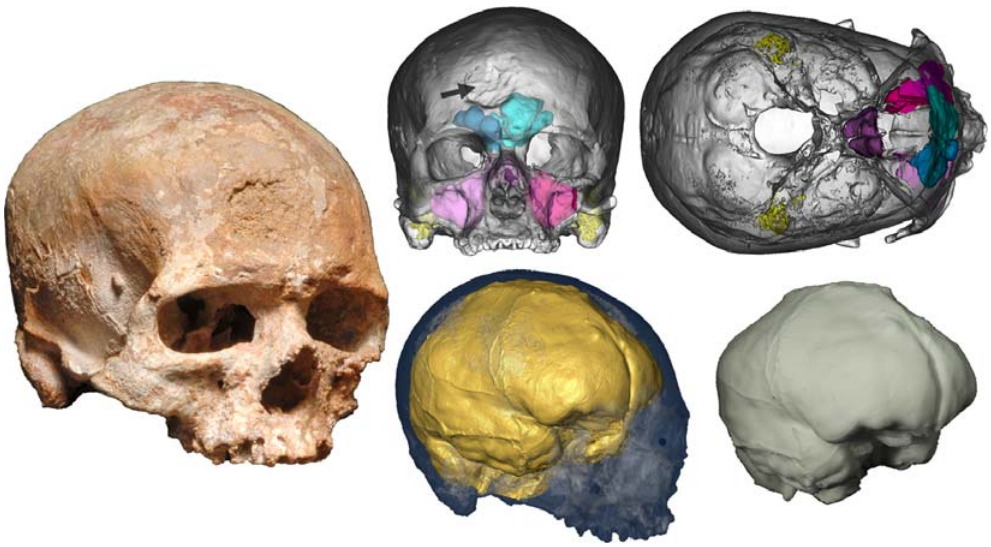

**Fig. 1** Anterolateral view of the original skull of Cro-Magnon 1; top row: illustration of its paranasal and temporal bone pneumatisation in the anterior and superior views, visible by transparency of the 3D model of the skull; the arrow indicates the position of the pathological alteration on the frontal squama; bottom row: visualisation of the 3D reconstruction of the virtual endocast, visible by transparency of the skull; physical replica of the endocast of Cro-Magnon 1 (A colour figure may be viewed in the online issue) / *Vue antérolatérale du crâne original de Cro-Magnon 1 ; la flèche indique la position de l'altération pathologique de l'écaille frontale ; ligne du haut : illustration de sa pneumatisation paranasale et de l'os temporal en vues antérieure et supérieure, visible par transparence du modèle tridimensionnel du crâne ; ligne du bas : visualisation de la reconstruction tridimensionnelle de l'endocrâne, visible par transparence du crâne ; réplique physique de l'endocrâne de Cro-Magnon 1 (une version en couleurs de la figure est disponible dans la version en ligne de l'article)*

Omo 2, Singa). In Asia, complete fossil skulls are rare. Some questions have been raised about the antiquity of the specimens from Liujang [24] and Zhoukoudian Upper Cave, whereas the Wajak fossil is dated to <8,000 BP [25]. Similarly, the chronology of the Australian specimens is debated, even though some of them are definitely ancient. However, the fossils from Coobool Creek, Kow Swamp, Lake Mungo, Naccurie and Willandra Lake cannot be considered in this study for various reasons such as incomplete preservation, availability of endocranial casts and intentional cranial deformation [26,27]. In the Levant, the Skhul and Qafzeh sites have delivered a large number of fossils, including some well-preserved skulls. Skhul V and Qafzeh 6 are well-preserved and are included in this study. These are the oldest specimens, aged 80,000 and 92,000 years respectively. Finally, European specimens have been more closely scrutinised in the past as more material was available, and more accessible to some extent, as well as being well-preserved. A large number of Upper Pleistocene endocasts have therefore been exhaustively investigated. This is the case, for example, of Cro-Magnon 3, Predmostí 3, 4, 9 and 10, Brno 3, Dolní Věstonice 1 and 2, from the oldest to the most recent specimen [1], or Cioclovina [28]. The ages of these specimens range from 35,000 to 25,000 years. Unfortunately, no information is available as yet about the endocast of Peştera cu Oase 2 [29], which is currently the oldest known directly dated well-preserved specimen, with an age of ≈35,000 $^{14}$C BP [30]. Cro-Magnon 1, with an age of c. 28,000 years [17], is therefore one of the oldest nearly complete endocasts of European fossil *H. sapiens* available to date, but it has never been described as yet.

The fossil remains discovered in the Cro-Magnon site are stored in the collections of the Musée de l'Homme in Paris, France. The skull of Cro-Magnon 1 (Fig. 1) was scanned with a 16-row CT scanner (LightSpeed 16; General Electric Medical Systems, Milwaukee, Wisconsin) [31]. Settings were 120 kV, 250 mA, 0.625-mm-thick slices, reconstruction interval of 0.4 mm, 23 cm field of view, 0.45 mm pixel size, 512 × 512 pixel matrix. Multiplanar reformatting, thresholding procedures, 3D volume rendering and metric analyses were performed with ArteCore 1 (NESPOS) and Avizo 7 (VGS). The boundary between the bone and the air as well as the limits of the different structures analysed were identified by manual segmentation. This protocol required the use of multiple threshold values as a function of variations in bone mineralisation. These settings enabled us to obtain precise outlines and limits of the endocranial cavity and of all

pneumatic cells corresponding to the different areas of pneumatisation, to produce accurate 3D reconstructions (see [32] for a complete discussion of the segmentation protocol and [33–35] for examples of applications to the reconstruction of virtual endocasts). Finally, we printed a 3D prototype of the Cro-Magnon 1 endocast (Fig. 1). The physical replica was used to produce classic descriptions and metric analysis of the endocast.

Comparative samples include physical endocasts of the collections of the Muséum national d'Histoire naturelle in Paris, France, and consist of several fossil AMH (Skhul V, Qafzeh 6, Cro-Magnon 3, Predmostí 3, 4, 9 and 10, Brno 3, Dolní Věstonice 1 and 2, from the oldest to the most recent specimen) and 102 endocasts of extant modern humans. The endocranial anatomy of Cro-Magnon 2, Mladeč 1 and Pataud 1 was also analysed with virtual models obtained from CT data. The 3D model of the Cioclovina endocast [28,36] was provided by Kranioti and also obtained from CT data. The fossil sample therefore comprises 15 fairly complete specimens ranging from 92 to 25 ka in age. Sex is unknown for most of the specimens because of the absence of associated infracranial elements and therefore of independent indicators for sexual identification. The individuals of the extant sample were non-pathological adults. The sex is not known for all the specimens of the sample, but the sex ratio is probably biased as this collection seems to comprise more males than females, at least for specimens whose sex is known. Most specimens are from recent historical times, with the majority from the last two centuries. The geographic origin of the specimens is diverse, as they include 39 Europeans, 24 from the Pacific area, 15 Africans, 13 Asians and 8 native Americans.

## Methods

### Morphology and morphometry of the endocast

Classic metric measurements using sliding and spreading callipers were performed on the physical endocasts, on virtual models with dedicated software (ArteCore and Avizo) and on drawings for dimensions quantified in projections. Values for Cro-Magnon 1 were obtained from the physical prototype obtained from the 3D reconstruction (Fig. 1). These measurements quantify the lengths, heights and widths of different areas of the endocast (Fig. 2 and Table 1, please refer to [1,37] for a complete description of the method).

The frontal, parietal and occipital chords were also quantified based on anatomical landmarks related to brain structures. The limit between the frontal lobes – located anteriorly – and the parieto-temporal lobes – located posteriorly – corresponds superiorly and medially to the junction of the central sulci and inferolaterally to the course of the small depressions towards the upper part of the Sylvian valley. This limit runs posteriorly to the coronal suture in a different direction, getting closer to the suture while approaching the Sylvian valley. The limit between the parieto-temporal lobes – located anteriorly – and the occipital lobes – located posteriorly – corresponds medially to the parieto-occipital sulcus, which is frequently identifiable anteriorly to the endo-lambda, and laterally to the pre-occipital notch. Overall, this limit follows the direction of the lambdoid suture but does not correspond exactly to its course. Imprinting of these sulcal impressions on fossil hominins is variable. They were identified and observed on the physical endocasts with grazing light and on the virtual models with virtual grazing light. A complete description and definition of the sulcal impressions is detailed elsewhere [1]. Figure 2 illustrates the position of these sulci and of the lobes they delimitate as well as of the major anatomical features described in this study. Finally, we also measured the surface of the frontal, parieto-temporal, occipital and cerebellar lobes [1,38]. The limits of the lobes were defined by drawing continuous sulci around closed areas (see [1] for a complete description of the methodology). These limits between the different lobes were distinguishable with enough confidence to be recognized independently by two of us. The coordinates of 3D landmarks (Fig. 2 and Table 1) for geometric morphometric analyses were registered with a microscribe [37]. However, the incomplete preservation of the fossil specimens prevented a detailed geometric morphometric comparison between the fossil and extant samples. These landmarks are also useful to define linear measurements (Fig. 2 and Table 1). Different morphometric and statistical procedures were applied to analyse the recorded data, using PAST 2.11 software [39]. Linear regressions were performed with the Reduced Major Axis algorithm [40], which minimises errors in both variables [41], and were used to investigate possible allometric effects in the recorded data. All morphometric data were scaled relatively to each individual's endocranial volume in order to limit bias in global brain size variation between samples. The cube-root of the endocranial volume (EV) for each individual was thus used for size correction for each linear variable ($(xi/(3\sqrt{EVi})*100)$) or for surface quantification ($((2\sqrt{xi})/(3\sqrt{EVi})*100)$). The coefficient of variation (CV = SD/mean) was corrected for small sample size using the parameter V* (Table 2), which is calculated as $V^* = [(1 + 1/4N) \times CV]$ [42,43]. The permutation *t*-test was preferred to the classic *t*-test to compare means for the fossil and extant AMH. This test uses the *t*-statistic but is non-parametric and is useful for comparing samples with non-normal distribution and of unequal size. The sequential Bonferroni procedure was used to correct for multiple tests [44,45].

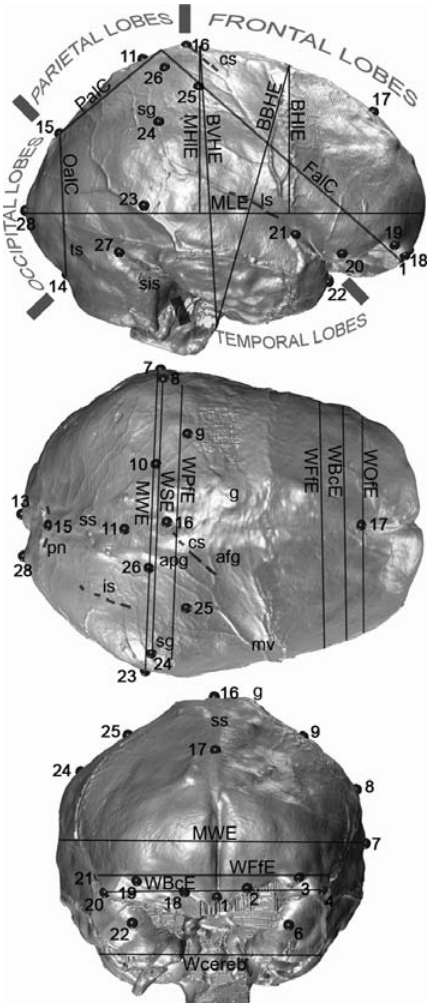


**Fig. 2** Three-dimensional model of the endocast of Cro-Magnon 1 in the right lateral, superior and anterior views showing the location of the landmarks and the measurements used to quantify the endocranial anatomy (the full list and definitions are given in Table 1) and the location of some analysed features (ss: sagittal sinus, ts: transverse sinus, sis: sigmoid sinus, mv: meningeal vessels, g: granular foveolas, cs: central sulcus, ls: lateral sulcus, is: interparietal sulcus, pn: pre-occipital notch, afg: ascending frontal gyrus, apg: ascending parietal gyrus, sg: supramarginal gyrus; see [1] for all illustrations and definitions) / *Modèles tridimensionnels de l'endocrâne de Cro-Magnon 1 illustrant la position des repères anatomiques et les mesures utilisées pour quantifier l'anatomie de l'endocrâne (leur liste complète et leur définition sont présentées dans le Tableau 1) et la position de caractères anatomiques (ss : sinus sagittal ; ts : sinus transverse ; sis : sinus sigmoïde ; mv : système méningé moyen ; g : granulations de Pacchioni ; cs : sulcus central ; ls : sulcus latéral ; is : sulcus interpariétal ; pn : scissure préoccipitale ; afg : gyrus frontal ascendant ; apg : gyrus pariétal ascendant ; sg : gyrus supramarginal ; et voir* [1] *pour l'ensemble des définitions et des représentations)*

## Mapping the asymmetries of the endocast

The asymmetries of the endocranial surface of Cro-Magnon 1, represented by a triangular mesh, were assessed through a three-step automated method:

- computation of the approximate plane of symmetry of the surface [46];
- computation of the 3D deformation field that allows the nonlinear registration of the endocranial surface with itself after mirror-flipping along its approximate plane of symmetry [47];
- and decomposition of each vector of this 3D deformation (subsequently termed "asymmetry") field into its 3 scalar coordinates in a right-handed Cartesian coordinate system consisting of the left–right, vertical and posterior–anterior axes.

Steps 1 and 2 were performed in a common statistical framework in which the mesh was modelled using a mixture of Gaussian probability density functions, and the points of the flipped mesh were considered as samples drawn independently according to this mixture; the plane of symmetry and field of asymmetry were considered as unknown parameters of the Gaussian mixture and were estimated using the maximum likelihood (ML) and the maximum a posteriori (MAP) principles, respectively; the ML and MAP estimations were performed using the Expectation–maximization (EM) algorithm [48].

The decomposition of each vector of the asymmetry field in an anatomy-based coordinate system allows a better interpretation of the asymmetric field: the posterior–anterior (PA) component shows whether one side protrudes more towards the front or the rear than the other, the vertical (top to bottom) component shows whether one side is higher or lower than the other, and finally the lateral (left to right) component shows whether one side is more or less laterally extended than the other with respect to the approximate computed plane of symmetry.

## Description of the internal cranial anatomy of Cro-Magnon 1

The external cranial anatomy of the specimen has been previously detailed by others [5,6,10,11]. However, the imaging dataset revealed that the internal structure of the bone is very well-preserved which previously allowed the quantification of cranial vault, tabular table and diploic layer thicknesses [32], as is the endocranial surface of the specimen.

## Pneumatisation

The complete extension of the frontal sinuses is preserved, except for the lowest part just above the frontoethmoidal suture

**Table 1** Definition of the landmarks and the measurements used to quantify endocranial variations between fossil and extant anatomically modern *Homo sapiens* (see Fig. 2 and refer [1,37] for a complete description of the method) / *Définition des points repères et des dimensions utilisés pour quantifier les variations de l'endocrâne entre les échantillons fossile et récent d'Hommes anatomiquement modernes (voir Fig. 2 et lire* [1,37] *pour une description complète de la méthode)*

| **Landmarks** | **Definition** |
|---|---|
| 1 | Base of encephalic rostrum between left and right first frontal convolution in the midsagittal plane |
| 2 and 18 | Left and right external edge of the encephalic rostrum |
| 3 and 19 | Left and right orbital part of the 3rd frontal convolution |
| 4 and 20 | Left and right point of maximal curvature of triangular part of the 3rd frontal convolution |
| 5 and 21 | Left and right upper point of the Sylvian valley (between the opercular part of the 3rd frontal convolution and the temporal lobe) |
| 6 and 22 | Left and right most anterior point of the temporal lobe (temporal pole) |
| 7 and 23 | Left and right euryon (corresponding to the maximal endocranial width, MWE) |
| 8 and 24 | Left and right point of maximal curvature of the supramarginal gyrus |
| 9 and 25 | Left and right anterior point of the interparietal sulcus (base of the 1st parietal convolution) |
| 10 and 26 | Left and right middle point of anterior edge of the 1st parietal convolution |
| 11 | Intersection between the postcentral sulci and the interhemispheric fissure |
| 12 and 27 | Left and right upper point between the temporal and cerebellar lobes (upper point of temporo-cerebellar excavation) |
| 13 and 28 | Left and right point of maximal curvature of the occipital lobe (occipital pole) |
| 14 | Posterior interhemispheric point (most depressed point of the torcular herophili) |
| 15 | Intersection between the left and right perpendicular sulci and the interhemispheric fissure |
| 16 | Intersection between the central sulci and the interhemispheric fissure |
| 17 | Middle point of the frontal chord |
| **Dimensions** | **Definition** |
| MLE | Maximal length |
| MWE | Maximal width (between 7 and 23) |
| WSE | Maximal width measured on the supramarginal gyri (between 8 and 24) |
| WPfE | Maximal width measured on the foot of the 2nd parietal convolutions |
| WBcE | Maximal width measured on Broca's cap (between 4 and 20) |
| WOfE | Maximal width measured on the orbital part of the 3rd frontal convolutions (between 3 and 19) |
| WFfE | Maximal width measured on the foot of the 3rd frontal convolutions |
| Wcereb | Maximal width of the cerebellar lobes |
| BBHE | Endobasion-endobregma height |
| BVHE | Endobasion-endovertex height |
| MHlE | Maximal height above the maximal length |
| BHlE | Height of endobregma above the maximal length |
| FalC | Frontal chord (between the base of encephalic rostrum and the intersection between the central sulci and the interhemispheric fissure) |
| PalC | Parietal chord (between the intersection between the central sulci and the interhemispheric fissure and the intersection between the precentral sulci and the interhemispheric fissure) |
| OalC | Occipital chord (between the intersection between the precentral sulci and the interhemispheric fissure and the posterior interhemispheric point) |

(Fig. 1). The sinuses are large, particularly on the left side, extending laterally above the orbital roof and posteriorly in the frontal squama. They are fan-shaped from their base towards their uppermost extension where the cells become individualised. The cells are separated by very thin septa, as are the two sinuses. A large and circular pathological alteration is visible on the external surface of the right side of the frontal squama, where it has deeply eroded the bone. As a result, the right frontal sinus is separated from the bottom of the lesion by a very thin layer of bone. Sphenoidal pneumatisation is complete except for its anterior extension. The left sinus is slightly larger than the right sinus. Most of the shape of the maxillary sinuses is discernible but their upper and medial limits as well as the lateral extent of the left sinus are altered due to

bone loss in the orbital floor, the lateral walls of the nasal cavity and part of the left maxillary arch. The sinuses are very similar in size and shape on both sides. Finally, temporal bone pneumatisation fills the mastoid process as well as the upper part of the petrous portion and has propagated slightly towards the rear and above the external auditory meatus.

## Description of the endocranial anatomy of Cro-Magnon 1

### Overall morphology

The entire cerebral surface is preserved, except for very small portions with incomplete bone preservation corresponding to the medial half of the left orbital lobe including the area posterior to the encephalic rostrum, and a small area at the medial course of the left central sulcus because of sediment incrustations that could not be removed virtually with sufficient precision (Fig. 2). Sulcal impressions and meningeal vessels are easily discernible thanks to the remarkably well-preserved endocranial surface. The endocast is ovoid in shape in the superior view. Its maximum width is in the medial part of the supramarginal gyri. The sagittal curvature is regularly convex in the lateral view.

### Vascular impressions

Concerning the venous sinuses, there is no evidence of the sphenoparietal sinuses. The superior sagittal sinus is visible between the frontal lobes where its width increases anteroposteriorly as far as the granular foveolas located in the posterior part of the first frontal convolutions. The relief of the sinus is less apparent posteriorly and again clearer from the granular foveolas located in the upper part of the ascending parietal gyri to the posterior extent of the parietal lobes. The sinus deviates laterally to the right into the right transverse sinus. This latter sinus deviates slightly in the direction of the right cerebellar lobe. The width of the sinus increases along its course. The right sigmoid sinus is in marked relief. The left transverse sinus appears in the area of the confluence of the sinuses. Its width and relief are less marked than on the right side.

Concerning the meningeal vessels, the common tract of the middle meningeal system is obvious on both sides on the inferior surface of the temporal lobes from where it enters the skull through the foramen spinosum. The middle meningeal system shows a similar pattern on both hemispheres. The common tract splits into three unequal branches on the superior temporal gyrus close to the temporal pole. The most anterior branch corresponds to the anterior branch of the middle meningeal system. This imprint is very short, disappears in the area of the Sylvian valley on the left hemisphere and shows some ramifications on the third frontal convolution on the right side. The largest branch runs vertically and splits into two equal rami at the temporal fossa. The corresponding anterior (or bregmatic) ramus runs close to the coronal suture with short anterior ramifications towards the frontal lobes and longer ramifications posteriorly that reach the mid-sagittal area of the endocast. The posterior (or obelic) ramus runs along the lateral sulcus on the parietal lobe. Some anastomoses appear in the area of the angular gyrus. Finally, the posterior (or lambdatic) branch arising from the common tract runs horizontally as far as the inferior temporal gyrus, then upwards close to the temporocerebellar valley. This branch splits into two rami that reach the upper part of the temporal lobe and the occipital lobe respectively, where both show some ramifications. This posterior branch has longer rami with more ramifications on the right hemisphere, and an obelic branch that joins the obelic branch originating from the bregmatic branch, where they form a number of anastomoses. Therefore, the anterior ramus covers the posterior part of the frontal lobe and nearly the whole parietal lobe, being more developed than the posterior ramus on the left hemisphere. The anterior ramus extends from the ascending frontal gyrus to the supramarginal gyrus, whereas the angular gyrus is covered by the posterior ramus on the right hemisphere. These two rami are equally developed on the right side.

### Sulcal and gyral imprints

On the frontal lobes, the transverse curvature is regularly convex in the anterior view, except where granular foveolas form a bulky relief in the interhemispheric area. This curvature is more circular at the level of the coronal suture and is flattened on both sides more anteriorly. The encephalic rostrum is very short and wide, with a small inferior projection. The right side of the rostrum is more convex and seems to be projected more anteriorly. The course of the precentral sulcus is not easily discernible, and might correspond to the depressed area situated behind the imprint left by the coronal suture. The width of the ascending frontal gyri is estimated at 25 mm. Short and deep depressions clearly delimit the three frontal convolutions on both sides. The relief on the third frontal convolution is more clearly delimited on the left side. The corresponding area on the right side has more diffuse borders and seems larger. The ascending and anterior rami delimit the triangular part on both sides. The latter is depressed by the cap incisure on the left hemisphere. The bulge in the area where the Brodmann area 45 would be located is in its inferior part and separated from the temporal pole by a very narrow space, particularly on the right side where the frontal and temporal lobes are almost in contact. The Sylvian valley is continued posteriorly by a clearly

visible lateral sulcus on both sides. The course of these sulci is linear and almost horizontal.

Concerning the temporal lobes, their height on both sides is identical from the pole to the parietooccipital sulcus. The superior temporal sulcus is the least apparent but it clearly delimits the superior temporal gyrus on both sides. Short and deep depressions clearly delimit the middle and inferior temporal gyri. The fourth and fifth temporal gyri are delimited along their whole length by several depressions. These two last sulci converge towards the pole on the left lobe and are parallel on the right lobe. The upper part of the left temporal pole is less voluminous than on the right side.

On the parietal lobes, the transverse curvature is very angular with the more lateral projecting points situated at the supramarginal gyri: the curvature is regularly convex from the base of the temporal lobes to the upper part of the inferior parietal gyrus. It then becomes concave due to a wide and shallow depression in the area of the interparietal sulcus. The superior parietal gyri form a wide and large bulge, where the relief of the superior sagittal sinus is visible all along the parietal lobes. Many granular foveolas are visible on both sides of this sinus. The central sulcus is not clearly discernible in its uppermost extension. Its medial part clearly delimits the ascending parietal gyrus from its base to the level of the superior parietal gyrus on both sides. The central and postcentral sulci are therefore discernible and their uppermost extension could therefore be determined. The width of the ascending parietal gyri is estimated at 25 mm. The interparietal sulcus is more obvious on the right side. The interparietal sulci delimit the superior parietal gyri whose width decreases anteroposteriorly. The borders of the supramarginal gyri are clearly discernible. This gyrus is circular in shape and markedly convex. The primary intermediate sulci form a shallow depression. The angular gyrus has a more apparent anterior limit on the right side but the angular gyri are in clear relief on both sides. The anteroinferior portion of the inferior parietal gyrus forms a circular swelling of similar size on both sides. The parieto-occipital sulcus is only apparent from the pre-occipital notch on both sides.

The occipital lobes are below the parietal lobes and the sagittal curvature at the junction of these lobes is regularly convex in the lateral view. The occipital lobes have a slight posterior projection and are triangular in shape. The three occipital gyri are clearly discernible on the right side whereas only the inferior occipital sulcus is visible on the left side.

The cerebellar lobes are below the temporal and occipital lobes, in a posterior position relatively to the cerebrum, and are ovoid in shape. The horizontal sulcus is formed by small depressions on both hemispheres. The interhemispheric space is wide. The space between the temporal and cerebellar lobes is wider on the left side. The narrower space on the right side is due to the larger size of the posterior part of the inferior temporal gyrus and to a larger sigmoid sinus on this side compared to the left side.

## Endocranial asymmetries

A pattern of right frontal-left occipital petalia (following the definition and methodology of [49]) is visible on this endocast (Fig. 3). Moreover, the right frontal pole is located 1.8 mm anteriorly to the left pole and the left occipital pole projects 1.1 mm behind the right one (following the definition and methodology of [50]). The left occipital lobe also protrudes medially on the right side of the mid-sagittal plane of the endocast when viewed from the top. The hemispheric length is approximately equal on both sides (R: 182 mm, L: 180 mm). The width of the frontal lobes is nearly the same on both hemispheres, whereas the area of the left parietotemporal lobe is larger on the left side. Various quantified heights are equal on both sides. The supramarginal and angular gyri are well delimited and their relief is similar on both sides (Fig. 3). The bulge in the area where the Brodmann area 45 would be located is larger on the right side, thus narrowing the Sylvian valley. In this area, the anterior and posterior rami of the central sulcus are clearer on the left hemisphere. The middle meningeal system, including the distribution of the ramifications and anastomoses, displays a similar pattern and development on both hemispheres (Fig. 3).

We were also able to quantify the asymmetries of the whole endocast by comparing its right and left sides. We divided the observed bilateral variation into three components in order to characterise the asymmetries in the three dimensions separately (Fig. 4). Width differences (X axis, or lateral variation) are particularly noticeable on the temporal lobes (towards the right except for the posterior part of the inferior temporal gyrus, which is more laterally projected on the left side) and in the area of the first frontal gyrus and the superior parietal gyrus (towards the left). The areas corresponding to the occipital poles have a more lateral extension on the right side than on the left side and the left side seems to bend towards the right. The most pronounced vertical asymmetries (Y axis) concern the first frontal gyrus and the superior parietal gyrus (the left side being higher than the right side) as well as the posterior part of the inferior temporal gyrus and the lower part of the occipital lobe (the right side being higher than the left side). Finally, variations in anteroposterior layout (or protrusions, Z axis) show that the right hemisphere has a more anterior position overall compared to the left hemisphere, particularly in the anterior part of the frontal lobes and temporal lobes, the posterior part of the inferior parietal gyrus and the occipital lobe.

The pattern of asymmetry of this endocast may therefore be summarised as follows (refer to the areas in darker colours on Figs 4, 5). The pattern of right frontal-left occipital protrusion is confirmed. The anterior part of the frontal

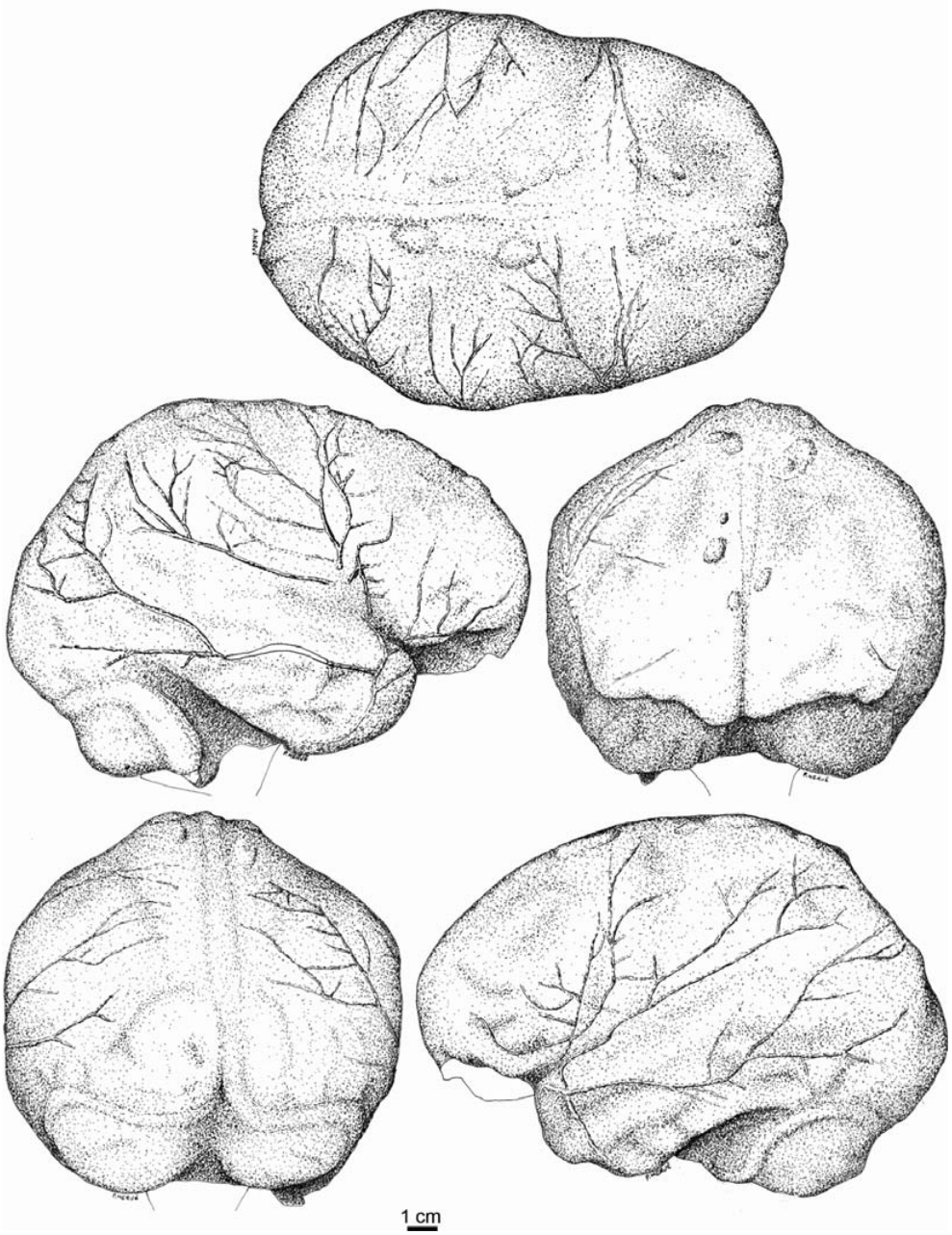


**Fig. 3** Line drawings of the endocast of Cro-Magnon 1 in the superior, right lateral, anterior, posterior and left lateral views; drawings by P. Hervé / *Dessins de l'endocrâne de Cro-Magnon 1 en vues supérieure, latérale droite, antérieure, postérieure et latérale gauche ; dessins de P. Hervé*

lobes is asymmetric only in the anteroposterior component, the right hemisphere being more anteriorly projected than the left one. The right occipital lobe (and its pole) is also more anterior than its counterpart on the other side, but is also in a more elevated position and more laterally expanded. The first frontal gyrus is asymmetric in its posterior half, as is the uppermost extension of the ascending frontal gyrus, the corresponding left gyri being more developed vertically and laterally than on the right side. The most asymmetric area of the parietal lobes is the superior parietal gyrus, which is higher and wider on the left hemisphere. The whole temporal lobe projects more laterally on the right side and also has a more anterior position.

## Comparative analyses of endocranial anatomy in *H. sapiens*

A comparison between fossil and extant *H. sapiens* is possible thanks to previous results [1] and to the original results and synthesis proposed here, which focus on features of

interest for the study of hominin evolution and/or features that vary among AMH.

### Vascular impressions

The superior sagittal sinus deviates into the right transverse sinus on all the fossil AMH where this region is preserved (Predmostí 3, 9, 10, Brno 3, Dolní Věstonice 2, Cro-Magnon 1, 3, Cioclovina) and on 80% of the extant humans. The right lateral sinus is larger and more marked than on the left on all the endocasts studied. No sphenoparietal sinus is observed among the 102 extant humans, and only Cro-Magnon 3 and Brno 3 exhibit a moderate relief in the corresponding area.

The middle meningeal system follows a similar pattern both on extant humans and the fossil AMH, with a predominant anterior ramus consisting of the bregmatic and obelic meningeal branches. The obelic branch has a double origin (from the bregmatic branch and from the lambdatic branch) on both hemispheres of Predmostí 3, on the right hemisphere of Predmostí 4 and on the left hemisphere of Dolní Věstonice 1 and 2. The anterior ramus is always more developed than the posterior (lambdatic) one, which is small on all the fossil AMH. The same pattern is observed in 80% of the extant humans, 12% of which have anterior and posterior branches with equivalent development. The anterior ramus covers the cerebral surface from the posterior region of the frontal convolutions to the angular gyrus on both sides on the extant humans, Cro-Magnon 3, Predmostí 10 and on the left hemisphere of Predmostí 9. On both sides on Cro-Magnon 1, Dolní Věstonice 1 and 2, Brno 3, Predmostí 3, 4, and on the right hemisphere of Predmostí 9, the anterior ramus is slightly less developed and reaches the supramarginal gyrus, and the angular gyrus is covered by the posterior ramus. The general orientation of the middle meningeal imprints is oblique. The ramifications are numerous and joined by a number of anastomoses that form a covering pattern. The ramifications and anastomoses are less numerous on fossil AMH than on extant humans.

### Sulcal and gyral imprints

Formed by the extremities of the left and right first frontal convolutions, the encephalic rostrum is short and wide on the fossil AMH and on the extant humans. The left convolution is wider on Predmostí 10, Cro-Magnon 3 and on 40% of

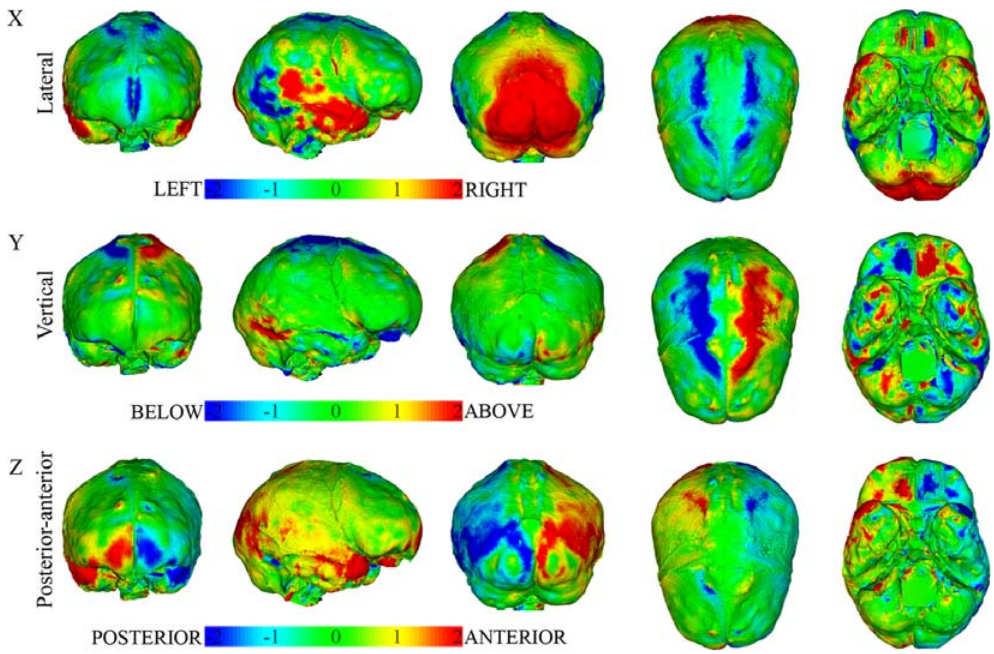


**Fig. 4** Illustration of bilateral asymmetries of the endocast of Cro-Magnon 1 in the anterior, right lateral, posterior, superior and inferior views, from left to right, in their lateral (X), vertical (Y) and posterior–anterior (Z) components. The chromatic scale highlights differences (from left to right sides of the scale) in lateral extension towards the left/right, vertical differences from bottom to top and horizontal differences from back to front (Colour figure may be viewed in the online issue) / *Illustration des asymétries bilatérales de l'endocrâne de Cro-Magnon 1 en vues antérieure, latérale droite, postérieure, supérieure et inférieure, de gauche à droite, détaillées dans leurs composantes latérale (X), verticale (Y) et antéropostérieure (Z). L'échelle chromatique illustre (de la gauche vers la droite de l'échelle) des différences latérales vers la gauche/droite, des différences verticales du bas vers le haut et des différences horizontales de l'arrière vers l'avant (une version en couleur de la figure est disponible dans la version en ligne de l'article)*

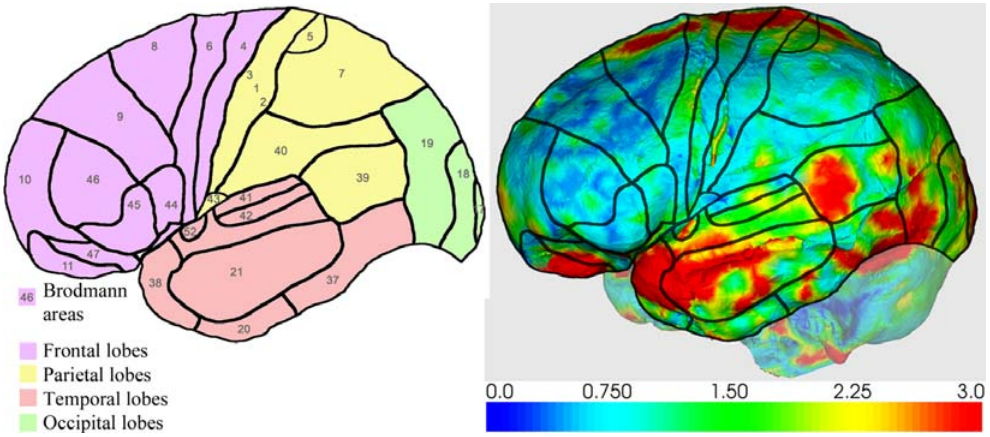


**Fig. 5** Illustration of the magnitude of the asymmetry vector made of the three components for the endocast of Cro-Magnon 1 and schematic superposition of Brodmann areas (Colour figure may be viewed in the online issue) / *Illustration du vecteur de symétrie combinant ses trois composantes pour l'endocrâne de Cro-Magnon 1 et superposition schématique des aires de Brodmann (une version en couleur de la figure est disponible dans la version en ligne de l'article)*

the extant humans. The right frontal convolution is wider on Predmostí 4, 9, Dolní Věstonice 1, 2, Cro-Magnon 1, Cioclovina and on 41% of the extant humans. The width of the extremities of these first frontal convolutions is identical on Predmostí 3 and on 19% of the extant humans. The left and right frontal hemispheres are nearly joined, separated only by a deep and narrow interhemispheric sulcus on all the endocasts studied. The frontal relief is marked and well delimited, especially on the third frontal convolution. The triangular part is perfectly delimited and more prominent and more bulging on the left hemisphere on Predmostí 4, Cro-Magnon 1, 3, Cioclovina and Dolní Věstonice 1. Incomplete preservation prevents comparison with the other fossil specimens. The left triangular part is also more developed on 72% of the extant humans (16% on the right lobe and 12% equal). The triangular part is depressed on all of them by the cap incisure. The triangular part is very close to the temporal pole, just separated by a narrow Sylvian valley. The frontal and temporal lobes are nearly joined. Posteriorly, the lateral sulcus is always deeply imprinted. It is rectilinear and nearly horizontal, and longer and deeper on the left hemisphere compared to the right.

The parietal gyri are well delimited, especially the large and convex first parietal convolution where the lower part is limited by the depressed interparietal sulcus. The relief on the second parietal convolution is also well marked, as is the supramarginal gyrus, which has a rounded shape. The bulge is more prominent on the left parietal lobe on Predmostí 3, Brno 3, Cro-Magnon 3 and Dolní Věstonice 2 than on 41% of the extant humans. The relief is more developed on the right parietal lobe on Predmostí 10 and on 37% of the extant humans. It is equally developed on both hemispheres on Predmostí 4, 9 and on 22 % of the extant humans.

The temporal sulci are parallel. On the fossil specimens, there is a wide space between the posterior part of the temporal and cerebellar lobes, which are located under the parietal and occipital lobes. The hemispheres and the cerebellar lobes are closer on extant humans, and the cerebellar lobes are in a more anterior position.

The occipital lobes on all the endocasts are in an anterior position, below the parietal lobes. They are widely separated on the fossil AMH and closer on extant humans: they are joined together in 30% of the specimens, separated by a deep and narrow fissure in half of the specimens and by a wider fissure in the remaining individuals.

## Morphometric analyses

The different dimensions quantified on the Cro-Magnon 1 endocast are within the range of variation observed in our sample of fossil modern humans. Therefore, we included Cro-Magnon 1 in the sample of fossil AMH (N = 8–15 depending on the variable analysed and the state of preservation of the specimens) and compared the latter sample with the sample of extant modern humans (N = 102).

The first important observation from this study concerns the endocranial volume. This volume is absolutely and significantly smaller in extant *H. sapiens* compared to the fossil sample ($p<0.001$). Moreover, a mean value of 1,350 $cm^3$ (SD = 77.5) was quantified on a sample of 20,000 recent skulls from all over the world, with some populational and geographic variations and sexual dimorphism [51]. Mean cranial capacity was 1,427 $cm^3$ (SD = 81.6) for males and 1,272 $cm^3$ (SD = 82.9) for females. The mean endocranial volume for a sample of 28 fossil specimens dated from

190,000 to 25,000 years, for which endocranial volume is documented [2], is 1,478 $cm^3$. The value obtained for our more limited fossil sample (N = 13) is 1,514 $cm^3$ (SD = 137.9). We do not have information on sex for the entire fossil sample but there is no reason to assume any significant over-representation of males and therefore any significant overestimation of the mean endocranial volume due to a sexual bias in the composition of the sample. Overall, these results suggest a decrease in endocranial volume between fossil AMH and recent humans, whatever their geographic origin [51].

For this reason, all data were scaled relatively to individual endocranial size in order to facilitate further comparisons between samples (Tables 2–4). Moreover, linear regressions between endocranial size and the scaled data for each quantified measurement were performed to detect any allometric relationships among the recorded morphometric data. For all the variables, the coefficient of regression was very low and the relationship was always non-significant.

The morphometric comparison between the fossil and extant samples brought out many common features, but also some significant relative metric differences (Table 2). The fossil sample is within the range of variation observed in the large sample of extant modern humans in most of the specimens analysed for morphometric data (Tables 2–4). Hotelling's T-squared test was used to test for differences between the fossil and extant samples, which are significant ($p<0.001$) when all the morphometric data are considered globally. Geometric morphometric analyses could not be performed on a large fossil sample because of the incomplete preservation of the specimens. A geometric morphometric test showed that the fossil specimens, including Cro-Magnon 1, were projected in the variation of the extant sample.

In more detail, the maximum length of the endocast (MLE) is significantly greater in the fossil sample (noted fossil AMH below) compared to the extant sample (noted extant AMH below) (15.9 versus 14.9, $p < 0.001$) and the difference between these mean values is 7%. Endocranial widths measured in different areas of the endocast (MWE, WSE, WPfE, WBcE, WOfE and WFfE located on different areas of the frontal and parietal lobes, Fig. 2 and Table 1)

**Table 2** Morphometric results for linear distances / *Résultats morphométriques pour les distances linéaires*

| | | EV (cr) | MLE | MWE | WSE | WPfE | WBcE | WOfE | WFfE | Wcereb | BBHE | BVHE | MHlE | BHlE |
|---|---|---|---|---|---|---|---|---|---|---|---|---|---|---|
| fossil | N | 15 | 13 | 14 | 15 | 14 | 12 | 9 | 11 | 9 | 9 | 8 | 11 | 12 |
| AMH | V* | 2.9 | 3.9 | 4.3 | 4.9 | 4.8 | 4.6 | 3.3 | 5.3 | 5.6 | 4.0 | 4.6 | 7,9 | 5,9 |
| | Min | 10.8 | 15.1 | 10.8 | 10.7 | 10.7 | 8.7 | 7.1 | 9.2 | 9.0 | 10.3 | 10.6 | 6,0 | 5,5 |
| | Mean-SD | 11.1 | 15.3 | 11.4 | 10.9 | 10.9 | 8.8 | 7.2 | 9.5 | 9.1 | 10.6 | 10.7 | 6,2 | 5,6 |
| | **Mean** | **11.5** | **15.9** | **11.9** | **11.4** | **11.4** | **9.2** | **7.5** | **10.1** | **9.7** | **11.0** | **11.2** | **6,8** | **6,0** |
| | Mean+SD | 11.8 | 16.5 | 12.3 | 12.0 | 12.0 | 9.7 | 7.7 | 10.6 | 10.2 | 11.4 | 11.7 | 7,3 | 6,3 |
| | Max | 12.0 | 17.0 | 12.9 | 12.5 | 12.5 | 10.0 | 7.9 | 10.9 | 10.6 | 11.8 | 12.2 | 7,8 | 6,5 |
| Extant | N | 102 | 102 | 102 | 102 | 102 | 102 | 102 | 102 | 102 | 101 | 101 | 101 | 101 |
| AMH | V* | 3.5 | 4.1 | 4.5 | 3.9 | 4.2 | 5.7 | 12.8 | 5.3 | 4.8 | 3.9 | 3.5 | 10,9 | 11,9 |
| | Min | 10.6 | 13.5 | 10.6 | 10.3 | 10.2 | 8.1 | 5.9 | 8.8 | 8.1 | 9.2 | 9.9 | 4,6 | 4,1 |
| | Mean-SD | 11.1 | 14.3 | 11.3 | 11.1 | 10.9 | 8.6 | 6.6 | 9.6 | 8.8 | 10.2 | 10.5 | 5,2 | 4,5 |
| | **Mean** | **11.5** | **14.9** | **11.9** | **11.5** | **11.3** | **9.1** | **7.5** | **10.1** | **9.2** | **10.6** | **10.8** | **5,8** | **5,1** |
| | Mean+SD | 11.9 | 15.5 | 12.4 | 11.9 | 11.8 | 9.7 | 8.5 | 10.7 | 9.7 | 11.0 | 11.2 | 6,4 | 5,7 |
| | Max | 12.5 | 16.0 | 13.1 | 12.7 | 12.4 | 10.5 | 9.9 | 11.5 | 10.3 | 11.5 | 11.8 | 7,5 | 6,8 |
| | **perm. t (bc) p** | **ns** | *** | **ns** | **ns** | **ns** | **ns** | **ns** | **ns** | * | * | * | *** | *** |
| | **% MeanVar** | **0** | **7** | **0** | **0** | **1** | **1** | **0** | **-1** | **5** | **4** | **3** | **16** | **16** |

N: number of individuals; V*: coefficient of variation corrected for small sample size; metric results with size correction; perm. t(bc) p: p value of the permutation t-test with sequential Bonferroni correction for multiple tests, * indicates a p-value < 0.05, ** $p < 0.01$, *** $p < 0.001$; %MeanVar: percentage of variation between the means for fossil AMH and extant AMH samples; see Fig. 2 for illustration of linear distances and Table 1 for definitions *(N : nombre d'individus ; V* : coefficient de variation corrigé pour des échantillons de petite taille ; les données présentées ont été corrigées pour la taille ; perm. t(bc) p : valeur p du test t de permutation avec correction séquentielle de Bonferroni pour tests multiples, * indique une valeur de $p < 0,05$, ** $p < 0,01$, *** $p < 0,001$; %MeanVar : pourcentage de variation entre les moyennes pour les échantillons fossile et récent d'Hommes anatomiquement modernes ; voir la Figure 2 pour illustration des distances linéaires et le Tableau 1 pour leurs définitions)*.

**Table 3** Morphometric results for the frontal, parietal and occipital chords / *Résultats morphométriques pour les cordes frontale, pariétale et occipitale*

| | | FC | PC | OC | Wfas | Wpas |
|---|---|---|---|---|---|---|
| fossil AMH | N | 14 | 15 | 14 | 12 | 12 |
| | V* | 4.03 | 6.79 | 8.11 | 18.67 | 12.15 |
| | Min | 10.59 | 5.17 | 5.25 | 1.46 | 1.46 |
| | Mean-SD | 10.88 | 5.60 | 5.47 | 1.58 | 1.61 |
| | **Mean** | 11.33 | 6.00 | 5.94 | 1.94 | 1.83 |
| | Mean+SD | 11.78 | 6.40 | 6.41 | 2.29 | 2.05 |
| | Max | 12.16 | 6.92 | 6.80 | 2.75 | 2.18 |
| Extant AMH | N | 102 | 102 | 102 | 101 | 101 |
| | V* | 4.34 | 11.03 | 8.65 | 12.53 | 12.61 |
| | Min | 9.48 | 4.58 | 4.12 | 0.83 | 0.83 |
| | Mean-SD | 10.22 | 5.72 | 4.66 | 1.11 | 1.13 |
| | **Mean** | 10.69 | 6.43 | 5.10 | 1.27 | 1.29 |
| | Mean+SD | 11.15 | 7.14 | 5.54 | 1.42 | 1.46 |
| | Max | 12.08 | 7.72 | 6.18 | 1.72 | 1.72 |
| | **perm. t(bc) p** | *** | * | *** | *** | *** |
| | **%MeanVar** | **6** | **-7** | **16** | **51** | **40** |

N: number of individuals; V*: coefficient of variation corrected for small sample size; metric results with size correction; perm. t(bc) p: p-value of the permutation t-test with sequential Bonferroni correction for multiple tests, * indicates a p-value < 0.05, ** p < 0.01, *** p < 0.001; %MeanVar: percentage of variation between the means for fossil AMH and extant AMH samples; see Table 1 for definitions of linear distances *(N : nombre d'individus ; V* : coefficient de variation corrigé pour des échantillons de petite taille ; les données présentées ont été corrigées pour la taille ; perm. t(bc) p : valeur p du test t de permutation avec correction séquentielle de Bonferroni pour tests multiples ; * indique une valeur de p < 0,05, ** p < 0,01, *** p < 0,001 ; %MeanVar : pourcentage de variation entre les moyennes pour les échantillons fossile et récent d'Hommes anatomiquement modernes ; voir le Tableau 1 pour la définition des distances linéaires)*.

are not significantly different between the two samples. The difference between the mean values for these variables for the two samples ranges from –1 to +2%. Only the width of the cerebellar lobes (Wecereb) is significantly greater in fossil AMH (9.7 versus 9.2, p<0.05, difference of 5%). Concerning endocranial heights, the different quantified dimensions (BBHE, BVHE, MHIE and BHIE, Tables 1, 2) are significantly larger in fossil AMH, with differences in mean values ranging from 3 to 16%. Partial heights above the maximum length of the endocast (MHIE and BHIE) vary to a much larger extent between fossil AMH and extant AMH (differences of 16%, p < 0.001) than do total heights (BBHE and BVHE, differences of 3–4%, p < 0.05).

The frontal chord and the occipital chord are significantly larger in fossil AMH (p < 0.001) whereas the parietal chord is significantly larger in extant AMH (p < 0.05, Table 3). In relation to this pattern, the width of the ascending frontal gyri (Wfas) and of the ascending parietal gyri (Wpas) are significantly (p < 0.001) larger in fossil AMH (N = 12, values of 1.94 for Wfas and 1.83 for Wpas) than in extant AMH (N = 101, 1.27 and 1.29).

Finally, the surface of the frontal lobe is significantly larger in fossil AMH (p<0.001), with a difference of 6% between the mean values of the samples, as is the surface of the occipital lobes (p<0.01) with a mean difference of 8%, whereas the surfaces of the parietal and temporal lobes are not significantly different (Table 4). The surface of the cerebellar lobes is significantly larger in extant AMH (p<0.05), with a mean difference of 5%.

The difference in shape between fossil AMH and extant AMH endocasts may therefore be described and summarised as follows. While the overall shape of the endocasts does not differ noticeably in lateral extension, the vertical and anteroposterior differences between the samples are significant. In extant AMH, the frontal lobes are relatively shorter anteroposteriorly and their surface is smaller. The parietal lobes are longer although the surface of the parietotemporal lobes does not change. The occipital lobes become shorter vertically and their surface is smaller. This is related to an anteroposterior compression of the endocast and to a vertical compression of its upper part, where the width does not differ between fossil AMH and extant AMH.

**Table 4** Morphometric results for the surface of the frontal, parieto-temporal, occipital and cerebellar lobes / *Résultats morphométriques pour la surface des lobes frontaux, pariétotemporaux, occipitaux et cérébelleux*

| | | Frontal lobes | Parietal lobes | Occipital lobes | Cerebellar lobes |
|---|---|---|---|---|---|
| fossil AMH | N | 11 | 7 | 10 | 7 |
| | V* | 4.3 | 5.0 | 6.1 | 6.4 |
| | Min | 109.9 | 133.7 | 68.6 | 62.6 |
| | Mean-SD | 115.6 | 134.3 | 70.0 | 63.2 |
| | **Mean** | 120.6 | 141.1 | 74.4 | 67.4 |
| | Mean+SD | 125.7 | 147.9 | 78.9 | 71.5 |
| | Max | 127.7 | 155.2 | 83.1 | 73.0 |
| Extant AMH | N | 98 | 98 | 98 | 97 |
| | V* | 4.0 | 2.9 | 8.0 | 5.4 |
| | Min | 100.4 | 129.3 | 53.9 | 61.5 |
| | Mean-SD | 109.3 | 136.1 | 63.2 | 67.3 |
| | **Mean** | 113.9 | 140.2 | 68.7 | 71.1 |
| | Mean+SD | 118.4 | 144.3 | 74.1 | 74.9 |
| | Max | 125.1 | 150.3 | 80.4 | 78.9 |
| | **perm. t(bc) p** | *** | **ns** | ** | * |
| | **%MeanVar** | **6** | **1** | **8** | **-5** |

N: number of individuals; V*: coefficient of variation corrected for small sample size; metric results with size correction; perm. t(bc) p: p value of the permutation t test with sequential Bonferroni correction for multiple tests, * indicates a p-value < 0.05, ** p < 0.01, *** p < 0.001; %MeanVar: percentage of variation between the means for fossil AMH and extant AMH samples *(N : nombre d'individus ; V* : coefficient de variation corrigé pour des échantillons de petite taille ; les données présentées ont été corrigées pour la taille ; perm. t(bc) p : valeur p du test t de permutation avec correction séquentielle de Bonferroni pour tests multiples ; * indique une valeur de p < 0,05, ** p < 0,01, *** p < 0,001 ; %MeanVar : pourcentage de variation entre les moyennes pour les échantillons fossile et récent d'Hommes anatomiquement modernes).*

## Discussion

### Cro-Magnon 1 and *H. sapiens*

"Virtual anthropology", with specific constraints related to the particular nature of the material analysed [52], is undoubtedly a useful addition to the large analytical toolkit available to researchers and curators. In the case of Cro-Magnon 1, imaging and prototyping methodologies have for the first time allowed the observation, reconstruction and physical reproduction of endocranial anatomical features (Fig. 1), which are helping to document the anatomy of this important specimen [5–7].

Frontal pneumatisation is highly variable in both extant (e.g., [53,54]) and fossil [17,32,55] *H. sapiens*. Cro-Magnon 1 is within this range of variation, whereas differences in shape and extension are obvious in this species compared with fossil hominins, and particularly Neandertals. However, as of now it is not clear whether the shape and size of the frontal sinuses can be really helpful to phylogenetic discussions. Moreover, their role and function also remain unclear [55,56]. Similarly, the pattern of temporal bone pneumatisation in Cro-Magnon 1 is within the range of variability described for *H. sapiens*, which differs to some extent from the characteristics observed in other hominin species [57,58]. Our previous works on temporal bone pneumatisation have shown that the development of pneumatisation does not play an active role in determining the morphology of the temporal bone, and particularly the expression of various apomorphic features of the different species. The development of temporal bone pneumatisation is likely to be principally related to available space and to the temporal bone morphology. In this context, the shape and distribution of the paranasal and temporal bone pneumatisation in Cro-Magnon 1 correspond to what would be expected for *H. sapiens*.

Finally, the endocranial morphology, including vascular, gyral and sulcal characteristics, of Cro-Magnon 1 is within the range of variation observed in *H. sapiens* [1], including both extant and fossil samples, which exhibit some clear differences with other hominin species [1,38]. However, we have also identified a number of differences between the sample of fossil AMH and our extant sample. These differences are discussed in more detail below.

## Endocranial asymmetries in *H. sapiens*

It was not possible to draw any firm conclusion on the presence of asymmetries at the populational level for fossil *H. sapiens* because of the restricted sample available. Values for Cro-Magnon 1 are larger than the mean values for the sample of extant modern humans but are within their range of variation. The largest asymmetry concerns the lateral component of the occipital petalia (cf. Fig. 4). Asymmetric areas are located in the anterior part of the frontal and temporal lobes, in the upper extension of the frontal and parietal lobes just laterally to the mid-sagittal plane, and concern the occipital lobes (Figs 4, 5). Cro-Magnon 1 shows similar patterns for all the components of endocranial petalia compared with a sample of 45 extant modern humans [50].

Human brain asymmetries have been documented for over a century and widely investigated for their functional, physiological or behavioural implications. For example, the larger frontal or occipital projection is usually coupled with a larger lateral extent of the more projecting hemisphere relative to the other. It is presently accepted that this pattern of asymmetry appeared with early *Homo* [2,49,59,60] and is most common in right-handed individuals [61–67]. Brain asymmetries are a topic in non-human primate studies [49,61,63,68–73] and are of special interest in paleoanthropology [1,2,49,59,60,74] because of their relationships with right and left handedness and, more generally, with specific aspects of human cognition, including language. However, the investigation of endocranial asymmetries in the human fossil record has not yet received the scrutiny it deserves. When all the available information about overall of the brain asymmetry in modern humans is considered, it appears that the left occipital lobe is significantly larger in volume [75], surface [38] and in the posterior extension of its pole [49,50] than the right occipital lobe. In the meantime, the right frontal lobe has a significantly larger volume [75], a non-significantly larger surface [37], a non-significantly larger anterior extension of its pole [50] and a more lateral extension [49]. Variations in morphology and size of the anterior part of the frontal lobe are related to variations in surface, particularly of the anterior extension, and probably to a lesser extent to variations in the volume of the whole lobe. This set of evidence from various studies and for different features shows that the occipital lobes exhibit a pattern of significant directional asymmetry in favour of the left side in the posterior extension at the population level in AMH, whereas variations in the shape and dimensions of the frontal lobes in our species seem to be mostly related to a pattern of fluctuating asymmetry. These aspects remain to be detailed from larger samples of fossil specimens, using new methodologies that allow fine details about brain asymmetries to be quantified. Recent results show that it is essential to define asymmetrical traits of the surface of the brain correctly by studying large populations with suitable methodologies. The methodology described here, which quantifies areas and directions of bilateral asymmetry, while remaining independent of overall brain asymmetry, will certainly allow major developments for the quantification of these features.

## Morphometric evolution of the *H. sapiens* brain

In detail, the analyses of the size-corrected variation described here show that the maximum length of the endocast is significantly larger in the fossil sample compared to the extant sample (Fig. 6). The widths and surfaces measured on different areas of the frontal parietal lobes do not differ significantly between the two samples, except for the width of the cerebellar lobes, which is significantly larger in Upper Pleistocene AMH. The different quantified endocranial heights are significantly larger in the fossil AMH sample. The frontal chord and the occipital chord are also significantly larger in the fossil AMH sample, whereas the parietal chord is significantly larger in the extant AMH sample. In relation to this pattern, the width of the ascending frontal gyri and of the ascending parietal gyri are significantly larger in the fossil AMH. Finally, the surface of the frontal and parietotemporal lobes are significantly larger in the fossil AMH, whereas the surface of the parietotemporal lobes does not differ significantly and the surface of the cerebellar lobes is significantly larger in the extant AMH sample. Although significant, this difference between the fossil and extant samples in the surface of the different brain regions is smaller than the differences observed between different species of the genus *Homo* [38]. Finally, we have demonstrated that the various reported differences between the fossil and extant samples were not correlated to size-related effects and not due to allometric effects: the linear regressions between endocranial size and the scaled data for each quantified measurement were all non-significantly correlated.

A decrease in absolute endocranial size since the Upper Pleistocene is noticeable in *H. sapiens*. Several hypotheses have been put forward to explain this decrease, and are yet to be fully explored. Although we cannot explain the origin of this variation as yet, we have also found that both extant and older endocrania have the same anatomical layout, but nonetheless show non-allometric differences in the relative size and organisation of different parts of the brain. Between the fossil sample and the extant *H. sapiens*, there is an overall decrease in the volume, relative length and height of the endocast, along with smaller frontal and occipital lobes, while the width of the endocast and the size of the parietal lobes has remained relatively stable and, finally, a relative expansion of the cerebellar lobes appears to have occurred (see also [76]). However, we cannot conclude on the possible differences in functionality of the brain related to these morphological variations as there is no evidence to support a clear discontinuity

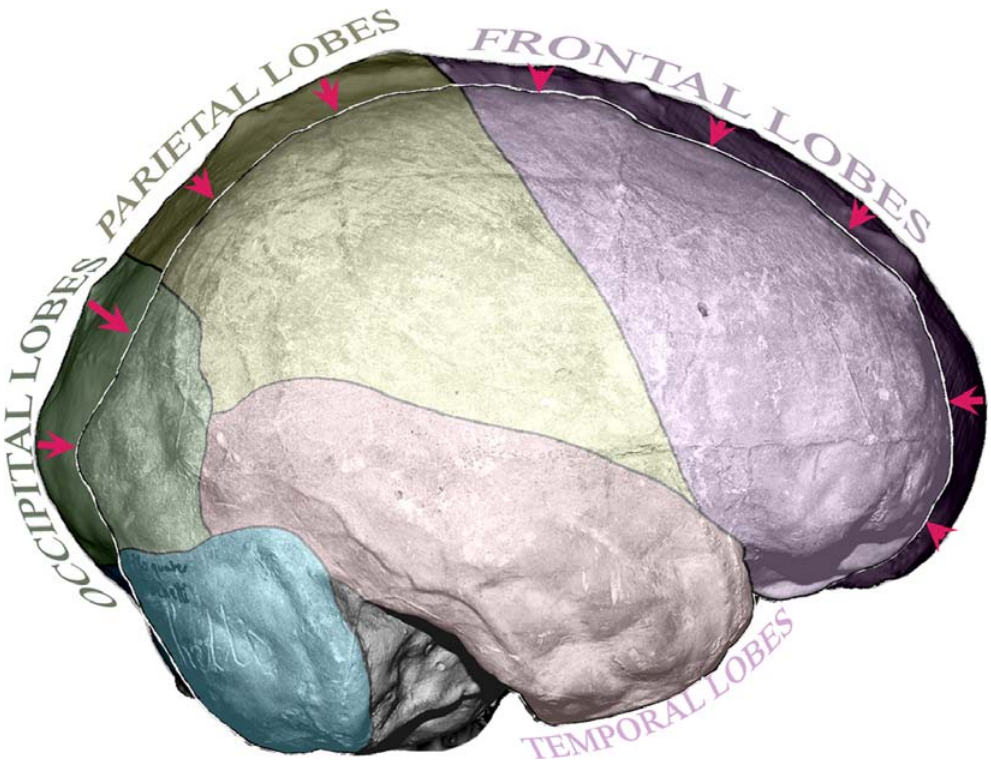


**Fig. 6** Schematic representation in the right lateral view of the variations in endocranial anatomy between a fossil (external outline corresponding to Cro-Magnon 1) and a "mean" extant anatomically modern human (internal outline corresponding to a recent endocast with quantified measurements made in this study that are close to the mean values for the extant AMH sample) (Colour figure may be viewed in the online issue) / *Représentation schématique en vue latérale droite de la variation morphologique de l'endocrâne entre les Hommes anatomiquement modernes fossiles (contour externe qui correspond à Cro-Magnon 1) et récents (contour interne qui correspond à un endocrâne d'Homme actuel dont les dimensions sont proches de la moyenne observée pour l'échantillon pour toutes les variables analysées (une version en couleur de la figure est disponible dans la version en ligne de l'article)*

between the capacities of our predecessors, Palaeolithic *H. sapiens*, and ours. The results we have obtained show that the *H. sapiens* brain is very plastic, with some areas (frontal and occipital lobes) being more adaptive than others (parietal, temporal or cerebellar lobes), which may be due to constraints on maintaining optimal performance while reducing in size and changing in shape.

## Conclusion

Developments in brain mapping and computational anatomy in the last twenty years have expanded possibilities for analysing brain structure and function (e.g. [77]). Here we have opened up a new perspective on knowledge of the anatomy of the *H. sapiens* brain, whose recent evolution had never before been investigated in the light of this feature, which is clearly an important gap in scientific knowledge.

A decrease in absolute endocranial size has occurred between fossil specimens and recent populations in *H. sapiens*. This variation is also associated with noticeable non-allometric variations in the relative size and shape of the different areas of the brain of fossil and extant AMH, which may be described and summarised as follows. The overall shape of the endocasts does not exhibit noticeable changes in width, but it does show substantial vertical and anteroposterior variations. The frontal lobes have become relatively shorter anteroposteriorly and their surface has decreased. Parietal lobes are longer while the surface of the parietotemporal lobes has not changed. Occipital lobes have become shorter vertically and their surface has decreased. This is related to an anteroposterior "compression" of the endocast and to a vertical "compression" of its upper part where its width does not differ between fossil and extant AMH. As of now, these morphological variations of the brain during the recent evolution of our species are impossible to correlate with functional data or interpretations of variations in human capacities that have certainly not varied so widely over time. This illustrates the complex correlation between form and function and highlights the considerable plasticity of the *H. sapiens* brain.

**Acknowledgments :** We are very grateful to the following institutions and individuals for allowing us to study endocasts in their care: E. Kranioti, University of Edinburgh, Scotland; A. Froment, P. Mennecier, H. de Lumley and F. Sémah, Muséum national d'Histoire naturelle, Paris, France. We are also indebted to A. Fort and V. Laborde for their help during the analysis of the endocast collection of the Musée de l'Homme and to P. Hervé for the drawings of the endocast of Cro-Magnon 1. This work has benefited from earlier discussions with E. Gilissen of the Royal Museum of Central Africa in Tervuren, Belgium. The comments from two anonymous reviewers and Editor in Chief E. Herrscher have greatly improved this paper.

## Bibliography

1. Grimaud-Hervé D (1997) L'évolution de l'encéphale chez *Homo erectus* et *Homo sapiens* : exemples de l'Asie et de l'Europe, Cahiers de Paléoanthropologie, CNRS, Paris, 406p
2. Holloway RL, Broadfield DC, Yuan MS (2004) The human fossil record: brain endocasts, paleoneurological evidence. Wiley, Hoboken, New Jersey, 315p
3. Sousa de A, Wood B (2007) The hominin fossil record and the emergence of the modern human central nervous system. In: Kaas JA (ed) Evolution of nervous systems: a comprehensive reference, Vol. 4: the evolution of primate nervous systems. Elsevier, Oxford, pp 291–336
4. Lartet L (1868) Une sépulture des troglodytes du Périgord. Bull Soc Anthropol Paris 3:335–49
5. Broca P (1868) Sur les crânes et ossements des Eyzies. Bull Soc Anthropol Paris 3:350–392
6. Broca P (1868) Description sommaire des restes humains découverts dans les grottes de Cro-Magnon près de Les Eyzies. Ann Sci Nat Zool Paléontol 10:145–55
7. Discussion collective (Bertillon, Pruner-Bey, Lagneau, Broca, Welcker, Hamy, de Mortillet, Gaussin, Bertrand, Halleguen, Girod) (1868) Sur les crânes et les ossements des Eyzies. Bull Soc Anthropol Paris 3:416–46, 454–514, 554–78
8. Quatrefages de A, Hamy E (1874) La race de Cro-Magnon dans l'espace et dans le temps. Bull Soc Anthropol Paris 9:260–6
9. Blanckaert C (2010) Les « trois glorieuses de 1859 » [Broca, Boucher de Perthes, Darwin] et la genèse du concept de races historiques. Bull Mem Soc Anthropol Paris 22:3–16
10. Vallois HV, Billy G (1965a) Nouvelles recherches sur les hommes fossiles de l'abri de Cro-Magnon. L'anthropologie 61:47–74
11. Vallois HV, Billy G (1965b) Nouvelles recherches sur les hommes fossiles de l'abri de Cro-Magnon. L'anthropologie 61:249–72
12. Gambier D (1986) Etude des os d'enfants du gisement aurignacien de Cro-Magnon, Les Eyzies (Dordogne). Bull Mém Soc Anthropol Paris 3:13–25
13. Pales L (1930) Paléopathologie et pathologie comparative, Masson, Paris
14. Dastugue J (1967) Pathologie des hommes fossiles de l'abri de Cro-Magnon. L'anthropologie 71:479–492
15. Thillaud PL (1981) L'histiocytose X au Paléolithique (sujet n°1 de Cro-Magnon), problématique du diagnostic ostéo-archéologique. L'anthropologie 85:219–239
16. Movius HL (1969) The abri of Cro-Magnon, Les Eyzies (Dordogne) and the probable age of the contained burials on the basis of the evidence of the nearby abri Pataud. Anur Estud Atlant 15:323–44
17. Henry-Gambier D (2002) Les fossiles de Cro-Magnon (Les Eyzies-de-Tayac, Dordogne), nouvelles données sur leur position chronologique et leur attribution culturelle. Bull Mém Soc Anthropol Paris 14:89–112
18. Henneberg M (1998) Evolution of the human brain: is bigger better? Clin Exp Pharmacol Physiol 25:745–9
19. Holloway RL (2008) The Human Brain Evolving: A Personal Retrospective. Ann Rev Anthropol 37(1):1–19
20. McDougall I, Brown FH, Fleagle JG (2005) Stratigraphic placement and age of modern humans from Kibish, Ethiopia. Nature 433:733–6
21. White TD, Asfaw B, DeGusta D, et al (2003) Pleistocene *Homo sapiens* from Middle Awash, Ethiopia. Nature 423:742–7
22. Crevecoeur I, Rougier H, Grine F, Froment A (2009) Modern human cranial diversity in the Late Pleistocene of Africa and Eurasia: evidence from Nazlet Khater, Peştera cu Oase, and Hofmeyr. Am J Phys Anthropol 140:347–58
23. Schwartz JH, Tatersall I (2010) Fossil evidence for the origin of *Homo sapiens*. Yrbk Phys Anthropol 143:94–121
24. Wu X, Wu L, Que J, Wang Y (2008) The brain morphology of *Homo* Liujiang cranium fossil by three-dimensional computed tomography. Chin Sci Bull 53:2513–19
25. Storm P (1995) The evolutionary significance of the Wajak skulls. Scripta Geologica 110:1–247
26. Détroit F (2002) Origine et évolution des *Homo sapiens* en Asie du Sud-Est : descriptions et analyses morphométriques de nouveaux fossiles, Ph.D. Dissertation, Muséum national d'Histoire naturelle, Paris, France, 444p
27. Antón SC, Weinstein KJ (1999) Artificial cranial deformation and fossil Australians revisited. J Hum Evol 36:195–209
28. Kranioti F, Holloway R, Senck S, et al (2011) Virtual assessment of the endocranial morphology of the early modern European fossil calvaria from Ciocliovina, Romania. Anat Rec 194:1083–92
29. Rougier H, Milota Ş, Rodrigo R, et al (2007) Peştera cu Oase 2 and the cranial morphology of early modern europeans. Proc Natl Acad Sci 4:1165–70
30. Trinkaus E, Moldovan O, Milota Ş, et al (2003) An early modern human from the Peştera cu Oase, Romania. Proc Natl Acad Sci 100:11231–6
31. Badawi-Fayad J, Yazbeck C, Balzeau A, et al (2005) Multidetector row CT scanning in Paleoanthropology at various tube current settings and scanning mode. Surg Radiol Anat 27:536–43
32. Balzeau A (2005) Spécificités des caractères morphologiques internes du squelette céphalique chez *Homo erectus*, Ph.D. Dissertation, Muséum national d'Histoire naturelle, Paris, France, 394p
33. Balzeau A, Jacob T, Indriati E (2002) Structures crâniennes internes de l'*Homo erectus* Sambungmacan 1 (Java, Indonésie). CR Palevol 1:305–310
34. Balzeau A, Grimaud-Hervé D, Jacob T (2005) Internal cranial features of the Mojokerto child fossil (East Java, Indonesia). J Hum Evol 48:535–53
35. Balzeau A, Gilissen E, Wendelen W, Coudyzer W (2009) Internal cranial anatomy of the type specimen of *Pan paniscus* and available data for study. J Hum Evol 56:205–8
36. Harvati K, Gunz P, Grigorescu D (2007) Cioclovina (Romania): affinities of an early modern European. J Hum Evol 53:732–46
37. Grimaud-Hervé D, Lordkipanidze D (2010) The fossil hominid brains of Dmanisi: D 2280 and D 2282. In: Broadfield D, Yuan M, Schick K, Toth N (eds) The human brain evolving: paleoneurological studies in honour of Ralph L. Holloway. Stone Age Institute Publication Series, Indiana, pp 59–82

38. Balzeau A, Holloway RL, Grimaud-Hervé D (2012) Variations and asymmetries in regional brain surface in the genus *Homo*. J Hum Evol 62:696–706
39. Hammer O, Harper DAT, Ryan PD (2001) PAST: Palaeontological Statistics Software Package for education and data analysis. Palaeontol Electron 4(1):9
40. Miller RL, Kahn JS (1962) Statistical analysis in the geological sciences. John Wiley & Sons, New York, 483p
41. Smith RJ (2009) Use and misuse of the reduced major axis for line-fitting. Am J Phys Anthropol 140:476–86
42. Sokal RR, Braumann CA (1980) Significance tests for coefficients of variation and variability profiles. Syst Zool 29:50–66
43. Wood B, Lieberman DE (2001) Craniodental variation in *Paranthropus boisei:* a developmental and functional perspective. Am J Phys Anthropol 116:13–25
44. Rice WR (1989) Analyzing tables of statistical tests. Evolution 43:223–5
45. Palmer AR (1994) Fluctuating asymmetry analyses: a primer. In: Markow TA (ed) Developmental instability: its origins and evolutionary implications. Kluwer, Dordrecht, Netherlands pp 335–64
46. Combès B, Hennessy R, Waddington J, Roberts N, Prima S (2008) Automatic symmetry plane estimation of bilateral objects in point clouds. IEEE Conference on Computer Vision and Pattern Recognition (CVPR'2008), June 2008, Anchorage, United States
47. Combès B, Prima S (2010) An efficient EM-ICP algorithm for symmetric consistent non-linear registration of point sets. 13th International Conference on Medical Image Computing and Computer-Assisted Intervention (MICCAI'2010), September 2010, Beijing, China
48. Dempster AP, Laird NM, Rubin DB (1977) Maximum likelihood from incomplete data via the EM algorithm. J Royal Stat Soc 39 (1):1–38
49. Holloway RL, de la Coste-Lareymondie MC (1982) Brain endocast asymmetry in pongids and hominids: some preliminary findings on the paleontology of cerebral dominance. Am J Phys Anthropol 58:101–10.
50. Balzeau A, Gilissen E, Grimaud-Hervé D (2012) Shared pattern of quantified endocranial shape asymmetries among anatomically modern humans, great apes and fossil hominins. Plos One 7(1): e29581
51. Beals KL, Smith CL, Dodd SM (1984) Brain size, cranial morphology, climate, and time machines. Curr Anthropol 25:301–30
52. Balzeau A, Crevecoeur I, Rougier H, et al (2010) Applications of imaging methodologies to paleoanthropology: beneficial results relating to the preservation, management and development of collections. CR Palevol 9:265–75
53. Tillier AM (1977) La pneumatisation du massif craniofacial chez les hommes actuels et fossiles. Bull Mem Soc Anthropol Paris XIII(4):177–189
54. O'Higgins P, Bastir M, Kupczik K (2006) Shaping the human face. Int Congr Ser 1296:55–73
55. Balzeau A, Badawi-Fayad J (2005) La morphologie externe et interne de la région sus-orbitaire est-elle corrélée à des contraintes biomécaniques ? Analyses structurelles des populations d'*Homo sapiens* d'Afalou Bou Rhummel (Algérie) et de Taforalt (Maroc). Bull Mem Soc Anthropol Paris 17:185–197
56. Zollikofer CPE, Ponce de León MS, Schmitz RW, Stringer CB (2008) New insights into mid-late Pleistocene fossil hominin paranasal sinus morphology. Anat Rec 291:1506–16
57. Balzeau A, Grimaud-Hervé D (2006) Cranial base morphology and temporal bone pneumatization in Asian *Homo erectus*. J Hum Evol 51:350–9
58. Balzeau A, Radovčić J (2008) Variation and modalities of growth and development of the temporal bone pneumatization in Neandertals. J Hum Evol 54:546–67
59. Holloway RL (1981) Volumetric and asymmetry determinations on recent hominid endocasts: Spy I and II, Djebel Ihroud I, and the Salé *Homo erectus* specimens, with some notes on neandertal brain size. Am J Phys Anthropol 55:385–93
60. Holloway RL (1981) The Indonesian *Homo erectus* brain endocasts revisited. Am J Phys Anthropol 55:503–21
61. LeMay M (1976) Morphological cerebral asymmetries of modern man, fossil man and nonhuman primate. Ann NY Acad Sci 280:349–66
62. LeMay M (1977) Asymmetries of the skull and handedness. J Neurol Sci 32:243–53
63. LeMay M, Billig MS, Geschwind N (1982) Asymmetries of the brains and skulls of nonhuman primates. In: Falk D, Armstrong E (eds) Primate brain evolution. Methods and concepts. Plenum Press, New York, pp 263–77
64. LeMay M, Kido DK (1978) Asymmetries of the cerebral hemispheres on computed tomograms. J Comput Assist Tomogr 2:471–6
65. Galaburda AM, LeMay M, Kemper TL, et al (1978) Right-left asymmetries in the brain. Science 199:852–6
66. Kertesz A, Black SE, Polk M, et al (1986) Cerebral asymmetries on magnetic resonance imaging. Cortex 22:117–27
67. Kertesz A, Polk M, Black SE, et al (1990) Sex, handedness, and the morphometry of cerebral asymmetries on magnetic resonance imaging. Brain Res 530:40–48
68. Falk D, Hildebolt C, Cheverud J, et al (1990) Cortical asymmetries in frontal lobes of rhesus monkeys (*Macaca mulatta*). Brain Res 512:40–45
69. Cain DP, Wada JA (1979) An anatomical asymmetry in the baboon brain. Brain Behav Evol 16:222–6
70. Cheverud J, Falk D, Hildebolt C, et al (1990) Heritability and association of cortical petalias in rhesus macaques (*Macaca mulatta*). Brain Behav Evol 35:368–72
71. LeMay M (1985) Asymmetries of the brains and skulls of nonhuman primates. In: Glick SD (ed) Cerebral lateralization in nonhuman species. Academic Press, New York, pp 233–45
72. Hopkins WD, Marino L (2000) Asymmetries in cerebral width in nonhuman primate brains as revealed by magnetic resonance imaging (MRI). Neuropsychologia 38:493–9
73. Pilcher DL, Hammock EAD, Hopkins WD (2001) Cerebral volumetric asymmetries in non-human primates: a magnetic resonance imaging study. Laterality 6:165–79
74. Tobias PV (1987) The brain of *Homo habilis*: a new level of organization in cerebral evolution. J Hum Evol 16:741–61
75. Geschwind DH, Miller BL, DeCarli C, et al (2002) Heritability of lobar brain volumes in twin supports genetic models of cerebral laterality and handedness. Proc Natl Acad Sci 99:3176–81
76. Balzeau A, Grimaud-Hervé D, Gilissen E (2011) Where are inion and endinion? Variations of the exo- and endocranial morphology of the occipital bone during hominin evolution. J Hum Evol 61:488–502
77. Toga AW, Thompson PM (2001) Maps of the brain. Anat Rec 265:37–53